JCI The Journal of Clinical Investigation

cGAS/STING axis mediates a topoisomerase II inhibitor-induced tumor immunogenicity

Zining Wang, … , Liang-ping Xia, Xiaojun Xia

J Clin Invest. 2019. https://doi.org/10.1172/JCI127471.

Research In-Press Preview Immunology Oncology

Graphical abstract

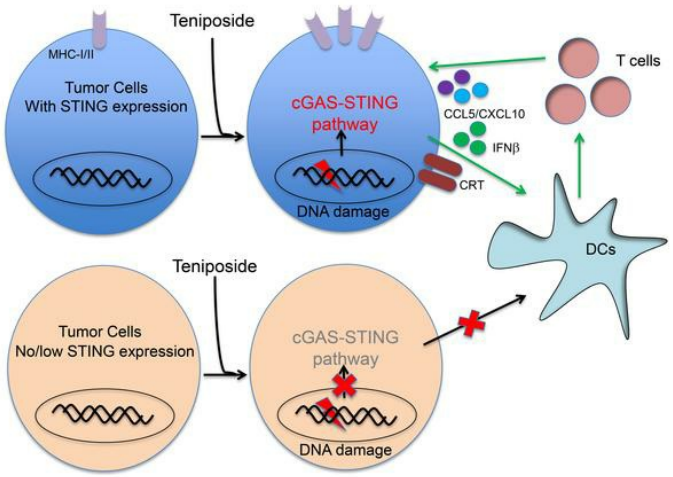

Title: cGAS/STING axis mediates a Topoisomerase II inhibitor-induced tumor immunogenicity

Authors: Zining Wang[1], Jiemin Chen[1], Jie Hu[2], Hongxia Zhang[1], Feifei Xu[1], Wenzhuo He[1], Xiaojuan Wang[1], Mengyun Li[1,3], Wenhua Lu[1], Gucheng Zeng[4], Penghui Zhou[1], Peng Huang[1], Siyu Chen[5], Wende Li[5], Liang-ping Xia[1,6*], Xiaojun Xia[1,7*]

Affiliations:

[1]State Key Laboratory of Oncology in South China, Collaborative Innovation Center for Cancer Medicine, Sun Yat-sen University Cancer Center, Guangzhou, China

[2]Department of Medical Oncology, The First Affiliated Hospital of Sun Yat-sen University, Guangzhou, China

[3]College of Food Science and Engineering, Northwest A&F University, Yangling, China

[4]Department of Microbiology, Zhongshan School of Medicine, Key Laboratory for Tropical Diseases Control of the Ministry of Education, Sun Yat-sen University, Guangzhou, China

[5]Guangdong Laboratory Animals Monitoring Institute, Guangdong key laboratory of laboratory animals, Guangzhou, China

[6]Department of Medical Oncology, Sun Yat-Sen University Cancer Center, Guangzhou, China,

[7]Lead Contact

*Address correspondence to:

Xiaojun Xia or Liang-ping Xia, State Key Laboratory of Oncology in South China, Sun Yat-sen University Cancer Center, 651 Dongfengdong Road, Guangzhou 510060, P. R. China Phone: +86-20-87343997; Email: xiaxj@sysucc.org.cn or xialp@sysucc.org.cn

Brief Summary:

By screening 1280 FDA-approved drugs, we identified a topoisomerase II inhibitor, tenoposide, which could kill cancer cells, trigger cancer immunogenicity, and potentiate the efficacy of anti-PD1 cancer immunotherapy by activating a cGAS/STING-dependent innate immune signaling.

Abstract:

Checkpoint blockade antibodies have been approved as immunotherapy for multiple types of cancer, but the response rate and efficacy are still limited. There are few immunogenic cell death (ICD)-inducing drugs available that can kill cancer cells, enhance tumor immunogenicity, increase the in vivo immune infiltration, and thereby boosting a tumor response to immunotherapy. So far, the ICD markers have been identified as the few immuno-stimulating characteristics of dead cells, but whether the presence of such ICD markers on tumor cells translates into enhanced antitumor immunity in vivo is still investigational. To identify anticancer drugs that could induce tumor cell death and boost T cell response, we performed drug screenings based on both an ICD reporter assay and T cell activation assay. We identified that teniposide, a DNA topoisomerase II inhibitor, could induce high mobility group box 1 (HMGB1) release and type I interferon signaling in tumor cells, and teniposide-treated tumor cells could activate antitumor T cell response both in vitro and in vivo. Mechanistically, teniposide induced tumor cell DNA damage and innate immune signaling including NF-κB activation and STING-dependent type I interferon signaling, both of which contribute to the activation of dendritic cells and subsequent T cells. Furthermore, teniposide potentiated the antitumor efficacy of anti-PD1 on multiple types of mouse tumor models. Our findings showed that teniposide could trigger tumor immunogenicity, and enabled a potential chemo-immunotherapeutic approach to potentiate the therapeutic efficacy of anti-PD1 immunotherapy.

[Main Text:]

Introduction

Cancer immunotherapy has become the major theme of cancer treatment regimens in the recent few years, testifying the genuine capability of the immune control of cancer (1-2). Among the few highly successful immunotherapeutic approaches, anti-PD1 antibody has demonstrated impressive efficacy across several different cancer types (3-4). Mechanistically, anti-PD1 or anti-PD-L1 blocking antibodies block the interaction between PD-L1/L2 and PD1 receptor and the immunosuppressive signal on T cells, thus restoring the antitumor function of exhausted T cells (5-7). Despite the prevalent success on different types of cancers, the response rate of anti-PD1 antibody therapy is quite low, ranging from 20% to 40%, and reliable biomarkers for predicting therapeutic response or efficacy is still lacking (2-3). Accumulating evidence suggests that the tumor response to anti-PD1 is highly dependent on tumor immunogenicity (i.e. tumor mutation burden, neoantigen abundance), intra-tumor PD-L1 expression, and an immune-active tumor microenvironment (8-11). Immunogenic cell death (ICD)-inducing drugs may enhance tumor antigen exposure, boost the release of immune-stimulating tumor cell content and elicit immune cell infiltration, thus converting the immune "cold" tumor into "hot" tumor. The combination of such drugs with immunotherapy, i.e. anti-PD1, may enhance the antitumor efficacy and expand the benefit of immunotherapy (12-13). Thus, identifying drugs that can both enhance tumor immunogenicity and potentiate tumor response to anti-PD1 therapy is significantly needed.

Recent studies have shown that some chemotherapeutic drugs could induce tumor cell ICD, which could potentially elicit or enhance an antitumor immune response (13-17). The common features of ICD are up-regulated expression or release of damage-associated molecular patterns (DAMPs) by the dying tumor cells (13). The release of HMGB1 and ATP could serve as

chemoattractant signals to recruit the antigen presenting cells (APCs), such as dendritic cells (DCs) and macrophages. Alongside, the membrane translocation of calreticulin (CRT) on the dying tumor cells serve as an “eat-me” signaling to promote phagocytosis or efferocytosis by the APCs, which process and present the tumor antigens to T cells (18-19). In addition, innate immune signaling activation such as Nuclear Factor-κB (NF-κB) pathway and type I interferon (IFN-I) signaling activation in dying tumor cells induces inflammatory cytokines，chemokines, and IFN-I production, which in turn promote DC maturation and T cell activation (13, 20-21). Accordingly, the dying tumor cells work as an in-situ vaccine by attracting APCs and inducing their activation and maturation to present tumor antigens to T cells, which subsequently undergo proliferation and attack tumor cells specifically (13). In this way, ICD-inducing chemotherapy drugs not only kill cancer cells but also activate anti-cancer immunity, which may potentiate the therapeutic efficacy of immunotherapy (22). However, all the known ICD markers do not always translate into strong in vivo antitumor immunity, and systemic evaluation of the ICD features of currently approved drugs have yielded inconsistent results due to tumor-intrinsic variation of capacities of some cellular functions such as autophagy or necroptosis (19, 23-24).

Currently, there are several reporter systems used for ICD inducer drug screening such as fluorescent biosensor of CRT-GFP or HMGB1-GFP, ATP, and ELISA measurement of HMGB1 (25). As cells undergo ICD, CRT will translocate from the perinuclear ER to cell surface, and HMGB1 will be released from the nucleus to the extracellular space. Such intracellular translocation can be tracked by the fused GFP fluorescent signal change that can be detected with a fluorescent microscopy (17). However, ICD features cannot be reflected by a single marker, thereby positive hits from one assay may not convincingly enhance tumor immunogenicity. Furthermore, the ICD phenotype of tumor cells may not always induce immune

cell activation. To accurately measure the drug-induced tumor immunogenicity, we designed a T cell activation assay as well as HMGB1- Gaussia luciferase (Gluc) reporter assay. In the T cell activation assay, T cells and DCs were co-cultured with tumor cells pre-treated with different drugs, and then T cell activation was measured by detecting extracellular IL-2 levels (detected by ELISA) or IL-2-promoter-driven β-galactosidase (LacZ) reporter gene activity. In the HMGB1-Gluc assay, the HMGB1 release, one hallmark of ICD, was detected by measuring HMGB1-fused Gaussia luciferase activity. By combining two screening assay results, we identified that the DNA topoisomerase II inhibitor, teniposide, was capable of eliciting tumor cell ICD and subsequent T cell activation. Further investigations revealed that teniposide could induce DCs and T cell activation, and protect against tumor growth when used in a vaccine setting. Teniposide could also upregulate the antigen presentation machinery on tumor cells. More importantly, teniposide induced the NF-κB and type I IFN pathway activation through the cGAS-STING axis, and potentiated DC-mediated antigen presentation to T cells. On both immunotherapy-sensitive and resistant mouse tumor models, teniposide promoted the tumor infiltration and activation of CD8+ T cells and boosted the antitumor efficacy of anti-PD1 therapy. Our findings suggested that teniposide could increase tumor immunogenicity, boost antitumor immunity, and provide a potential chemo-immunotherapeutic approach for cancer treatment by teniposide in combination with anti-PD1 antibody.

Results

Combined drug screening assays identified teniposide as an ICD drug

ICD drug screening has been reported by several groups, but so far, the known ICD markers cannot directly reflect the T cell activation induced by dead tumor cells. To circumvent this issue, we adapted an antigen presentation assay to directly examine the T cell activation upon tumor cell death. We treated ovalbumin (OVA)-expressing B16 mouse melanoma cells (B16-OVA) with an FDA-approved drug library for 16 hours, co-cultured with bone marrow-derived DCs (BMDCs) and OVA-specific CD8 T cell hybridoma B3Z cells for 24 hours, then measured the IL-2 promoter-driven LacZ activity which reflected the IL-2 expression (Figure 1A). Among the 1280 drugs tested, we identified a few drugs that could activate LacZ activity in B3Z cells in this assay (Table 1). To corroborate the results, we also designed an HMGB1-Gluc reporter assay to screen for drugs that could elicit the release of HMGB1, which is one of the hallmarks of ICD. In this HMGB1-Gluc reporter assay, HMGB1 was fused with a Gaussia luciferase (Gluc) and drug-induced HMGB1-Gluc release elicited luciferase activation (Figure 1B and Supplementary Figure S1A-C). In this reporter assay, acrisorcin and teniposide induced the highest level of HMGB1-Gluc activation above the basal level (Table 1). As teniposide was the only FDA-approved anti-neoplastic drug that we identified from both screening assays, we chose to focus on this drug for the subsequent experiments.

Teniposide is a Topoisomerase II (Top II) inhibitors currently used for treating several types of cancer including child acute lymphocytic leukemia. Interestingly, a few Top II inhibitors such as mitoxantrone and doxorubicin have been previously identified as a prototype of drugs eliciting cancer cell ICD features (18). We, therefore, compared the capabilities of these topoisomerase inhibitors for activating the HMGB1 release. Among the 6 inhibitors tested,

teniposide elicited the highest HMGB1-luc activity (Figure 1C). As drug-induced chemokine CXCL10 release has been recently considered as a new ICD marker, we measured the CXCL10 expression in cancer cells after treatment with the topoisomerase inhibitors. Consistently, teniposide was found to be able to induce the highest CXCL10 expression in both B16 mouse melanoma cells and MC38 mouse colon cancer cells (Figure 1D).

Teniposide induces tumor cell immunogenic cell death

The ability of teniposide to stimulate cancer cell ICD was then investigated. Teniposide treatment induced HMGB1-luc activity in a dose-dependent fashion (Figure 2A and Supplementary Figure S2A-B). Moreover, it also induced tumor cell death, which was detected by flow cytometry and LDH release (Figure 2B and Supplementary Figure S2C-D) and surface expression of calreticulin (CRT), another known ICD marker (Figure 2C and Supplementary Figure S2E). When mice bearing CT26 tumors were treated with teniposide, CRT expression levels in tumor tissues also increased (Supplementary Figure S2F). To unambiguously validate the in vivo effect of the tumor immunogenicity elicited by teniposide, we examined the immunogenicity of teniposide-treated tumor cells in a vaccination setting (26). We treated CT26 tumor cells with teniposide in vitro and injected the dead cells into the left flank of immunocompetent Balb/c mice. The mice were then re-challenged with live CT26 cells inoculation into the right flank 8 days later. A 100% tumor-free survival among mice immunized with teniposide-treated dead tumor cells in the 30 days post-challenge was observed, while all the mice that vaccinated with freeze-thawed tumor cells developed tumors (Figure 2D). As a comparison, vaccination with tumor cells pretreated by another Top II inhibitor, etoposide, only showed partial and temporary protection against tumor growth from live tumor cell rechallenge in such setting. These results together confirmed teniposide as a bona fide ICD inducer.

Teniposide upregulated the expression of tumor cell antigen presentation machinery

As tumor antigen expression on the tumor cell surface is essential for T cell recognition and killing, we investigated the influence of teniposide on the expression of tumor antigen presentation machinery components. Teniposide treatment increased MHC-I and MHC-II expression on the tumor cell surface (Figure 3A-B). Specifically, genes encoding mouse β2m (B2m), an essential component of the major histocompatibility complex (MHC) class I, was upregulated in teniposide-treated tumor cells, as were the genes directing peptide cleavage (Erap1), peptide transporters (Tap1 and Tap2), and transporter–MHC interactions (Tapbp) (Figure 3C). Furthermore, teniposide treatment increased the surface expression of MHC class I-bound SIINFEKL (OVA epitope peptide) complex on OVA-expressing mouse tumor cell lines (B16-OVA and MC38-OVA) (Supplementary Figure S3A). Ex vivo analysis of CT26 tumors also verified increased levels of MHCI, MHCII, and antigen presentation machinery gene expression after teniposide treatment (Supplementary Figure S3B). Taken together, teniposide was found to have the potential to enhance the expression of tumor antigen presentation machinery molecules.

Tumor cell treated with teniposide induces T cell activation and DC activation

We next determined the activation of T cells and DCs when they were co-cultured with teniposide-treated tumor cells. We treated B16-OVA cells with DMSO vehicle or teniposide for 20 hours, then co-cultured with BMDCs and B3Z T cells for 24 hours. Consistent with the increased LacZ activity (Figure 4A), the supernatant levels of T cell-derived cytokines IL-2 and IFNγ significantly increased in T cells co-cultured with tumor cells pre-treated with teniposide (Figure 4B-C). Meanwhile, the proportion of T cells expressing the activation marker CD69 and effector molecule granzyme B (Gzm B) also increased after co-culture (Figure 4D,

Supplementary Figure S4A). Similar results were obtained when primary OT-I T cells were used instead of B3Z cells (Figure 4E-G, Supplementary Figure S4B). Collectively, these data demonstrate that teniposide could boost the T cell activation. As DCs play a key role in the recognition of DAMPs associated with ICD and the subsequent uptake and presentation of tumor antigens to T cells, we next examined the activation status of DCs co-cultured with teniposide-treated tumor cells. Teniposide-treated B16 or MC38 tumor cells co-culture markedly increased the surface expression of activation markers including CD80, CD86, MHC-I, MHC-II, and CD40 on BMDCs (Figure 4H-L, Supplementary Figure S4C). Moreover, the surface expression level of MHC class I-bound SIINFEKL complex also significantly increased (Figure 4M). These data showed that teniposide-killed tumor cells induced BMDC maturation, antigen presentation, and subsequent T cell activation.

Teniposide induces tumor cell immunogenicity by activating NF-κB and Type I interferon signaling

Recent studies have shown that certain chemotherapy or irradiation could induce tumor cell DNA damage, cell death and inflammatory response, which could subsequently activate antitumor immunity depending on specific context (12, 27-28). DNA damage marker γ-H2AX expression was detected in tumor cells after teniposide treatment (Figure 5A, Supplementary Figure S5A). Consistently, genomic DNA was detected in cytoplasm after teniposide treatment (Supplementary Figure S5B). Interestingly, teniposide induced highest level of genomic DNA leaked in cytoplasm among the few inhibitors tested. At molecular level, both phosphorylated and total STAT1 protein levels were found to increase after teniposide treatment (Supplementary Figure S5C), indicating an IFN-I signaling activation. Interestingly, cGAS protein level also increased after teniposide treatment (Supplementary Figure S5D). Meanwhile, NF-κB signaling

was also activated, evidenced by increased level of p65 phosphorylation (Supplementary Figure S6A). As a consequence of the IFN-I and NF-κB activation, significant increase in mRNA and protein levels of downstream cytokines, CCL5 and CXCL10, were detected in B16, CT26, MC38 cells and in tumor tissues after teniposide treatment (Figure 5B-C, Supplementary Figure S5E-G).

The cGAS-STING pathway has been previously shown to be able to sense and respond to cytoplasmic or micronuclei DNA damage escaped from the nucleus (29-30). To investigate the role of this pathway in IFN-I activation, we generated *Sting*$^{-/-}$ B16 and MC38 cell lines using the CRISPR/Cas9 gene knockout technique and confirmed that the STING protein expression was absent in these cells (Supplementary Figure S5I). The knockout of STING abolished teniposide-induce IFN-I pathway activation (Figure 5D, Supplementary Figure S5H). More importantly, IL-2 production and CD69 expression on T cells were markedly attenuated when co-cultured with teniposide-treated *Cgas*$^{-/-}$ and *Sting*$^{-/-}$ B16-OVA cells as compared to that of T cells co-cultured with teniposide-treated WT B16-OVA cells (Figure 5E-F). Interestingly, tumor cells pre-treated with IKK inhibitor BAY-117082, or transduced with shRNA targeting IKKβ, also induced significantly lower levels of T cell activation upon teniposide treatment (Supplementary Figure S6B-D). Knock-down of TBK1 or IRF3 expression by gene-specific shRNAs partially inhibited T cell activation (Supplementary Figure S6E, F). In comparison, the pretreatment of tumor cells with inhibitors blocking RIPK1 (Nec-1), JNK (SP600125), ROS (NAC) or caspase (zVAD-FMK) did not have any effect on T cell activation (Supplementary Figure S6G). Thus, both NF-κB and cGAS/STING signaling are required for teniposide-induced tumor immunogenicity. To confirm that IFN-I activation in tumor cells could contribute to the DC function, we then treated B16-OVA cells with teniposide and co-cultured them with WT or *Ifnar*$^{-/-}$ BMDCs together with B3Z

cells. We observed significantly attenuated LacZ activation, IL-2 and IFNγ secretion in B3Z cells co-cultured with *Ifnar*$^{-/-}$ BMDCs (Figure 5G-I). These results together suggest that teniposide could induce NF-κB and cGAS-STING pathway-dependent IFN-I signaling activation in tumor cells, which in turn activate DCs and T cells.

Teniposide sensitizes tumor response to anti-PD1 treatment

Our observations indicated that teniposide could enhance the immunogenicity of tumor cells, which prompted us to examine the impact of teniposide treatment on the tumor microenvironment. Treatment with teniposide demonstrated significant tumor growth inhibition in CT26 and B16 tumor models (Figure 6A-B, Supplementary Figure S7A). By flow cytometry analysis of single cells isolated from tumor tissues, we found that teniposide treatment increased the percentage of tumor-infiltrating T cells and the number of tumor-infiltrating $CD8^+$ T cells, but not that of $CD4^+$ T cells (Figure 6C-E). A similar trend was observed as the $CD8^+$ T cell infiltration in B16, MC38 and PDAC pancreatic tumor model was found to increase (Supplementary Figure S7A-B). Moreover, a higher proportion of tumor-infiltrating T cells in the treatment group expressed the T cell activation marker CD69 and effector molecules Granzyme B and IFNγ, but not TNFα, as compared with the control group (Figure 6F-J, Supplementary Figure S7C). Tumor tissue-derived dendritic cells showed increased levels of MHC-I, MHC-II, CD40, and CD86 after teniposide treatment (Figure 6K-N). Importantly, CD8+ T cells are required for antitumor efficacy of teniposide, as pretreatment with anti-CD8 depletion antibody, but not anti-CD4 depletion antibody, abolished teniposide-induced CT26 tumor inhibition on Balb/c mice (Figure 6O).

Interestingly, teniposide also increased the PD-L1 surface expression on tumor cells (Supplementary Figure S7D). As intra-tumor PD-L1 expression and T cell infiltration are the two

major hallmarks of tumors responding to anti-PD1 therapy in the clinic (3), we next tested the therapeutic efficacy of combing teniposide with anti-PD-1 treatment on CT26 tumor model, which contains *K-Ras G12D* mutation and is known as not sensitive to checkpoint blockade antibody therapy (31). Mice with established subcutaneous CT26 tumors were treated with teniposide and anti-PD1 antibody alone or in combination. Teniposide treatment partially inhibited tumor growth, and teniposide in combination with anti-PD1 achieved the best tumor growth inhibition (Figure 6P). A similar result was observed in the MC38 and PDAC tumor mouse models (Supplementary Figure S7E). Strikingly, when STING expression was knocked down by shRNA in CT26 cells, the therapeutic efficacy of teniposide alone or in combination with anti-PD1 was markedly impaired, further supporting that teniposide-induced tumor immunogenic cell death and antitumor immunity was dependent on tumor-intrinsic STING activation (Figure 6Q, Supplementary Figure S7F). Collectively, these results showed that teniposide could induce immunogenic tumor cell death and activate the immune cells inside the tumor microenvironment, which may pave the way for the enhanced efficacy of anti-PD1 therapy on different tumor types.

Discussion

The known parameters reflecting ICD include the translocation of CRT, secretion of ATP, the release of HMGB1, and the recently added IFN-I and CXCL10 (13, 19). However, these markers only represent the hallmark changes on tumor cells, but do not directly reflect or guarantee immune activation. Thereby, the "gold standard" to validate the ICD features of a drug is in vivo vaccination using such drug-treated tumor cells (13). Such in vivo tests generate more reliable results but are often intensively laborious. Moreover, some of the ICD features rely on the functional capacity of specific intracellular signaling pathways such as ER stress or necroptosis pathway that are required for in vivo tumor immunogenicity (23, 32). However, various cancer cell lines may have defect in one or many of these pathways, and may not always derive consistent results in testing immunogenicity. Therefore, direct measurement on immune cell activation could circumvent the variation and uncertainty from measurements of markers on tumor cells. In this study, we adapted an antigen presentation assay to measure T cell activation induced by drug-treated tumor cells. In combination with a report assay measuring the release of HMGB1, a prototype ICD marker, we identified teniposide, a topoisomerase II inhibitor, as a candidate ICD inducer. Indeed, in vivo vaccination experiment validated the capacity of teniposide as a bona fide ICD drug.

Interestingly, a number of topoisomerase II inhibitors have been identified as ICD drugs, including mitoxantrone and doxorubicin (18). A liposomal form of irinotecan, a topoisomerase I inhibitor, was recently identified as an antitumor drug enhancing efficacy of T cell-based cancer immunotherapy (33). However, other topoisomerase inhibitors including camptothecin and etoposide did not elicit tumor cell ICD in our and others assay (25). Thus, topoisomerase II protein dysfunction per se is unlikely the original trigger of immunogenicity. On the other hand,

many chemotherapeutic drugs including topoisomerase inhibitors induced DNA damage in tumor cells, but most of them do not elicit tumor ICD, suggesting that DNA damage is insufficient to induce ICD features. Instead, recent findings suggest that the downstream innate immune signaling activation following DNA damage is more pertinent to tumor cell immunogenicity, such as NF-κB and IFN-I signaling (20, 27-28).

IFN-I signaling activation has been recently considered as a key feature of ICD (13). It is known that increased IFN-I not only enhance the immunogenicity of tumor cells, such as promoting antigen presentation but also regulate the tumor microenvironment by recruiting and activating DCs and antitumor T cells (34). The IFN-I pathway expression signature has been linked to positive prognosis in response to chemotherapy (21, 35-36). Treatment of various tumor types with the anthracycline class of chemotherapy induces cancer cell-autonomous IFN-I activation, which is dependent on tumor TLR3 and contribute to chemotherapy efficacy (21). Radiation therapy could also induce IFN-I in the tumor microenvironment, which in contrast, is dependent on the cGAS-STING pathway in DCs (27, 37). Direct intra-tumor injection of STING agonists boosted tumor immunogenicity (38-39), and in such scenario, tumor-intrinsic STING expression seemed less critical, but STING expression in APCs was more important for ensuing antitumor immunity (40). Similarly, oxaliplatin combined with cyclophosphomide boosted tumor immunogenicity through stromal myeloid TLR4 signaling (12). Our result suggests that tumor-intrinsic STING expression is essential for the enhanced antitumor therapeutic efficacy when using teniposide in combination with anti-PD1. Consistent with our finding, a recent study reported that a PARP inhibitor activated tumor cell-intrinsic STING pathway to promote DC activation and T cell recruitment in BRCA1-deficient triple negative breast cancer tumor models (41). The discrepancy about the role of stroma activation following chemotherapy or irradiation

therapy may derive from different treatment regimens or tumor models, but it is most likely that the innate immune signaling including NF-κB and IFN-I pathway activation would involve both cancer cell-intrinsic sensitivity and stroma activation, especially when combined with immunotherapy. Our finding highlight an essential role of tumor-intrinsic STING expression for tumor response to chemo-immunotherapy using DNA damaging agents such as teniposide. As STING expression is often dysregulated in human cancers (42), an immunohistochemical test of intratumoral STING expression may help predict patient response to such combination treatment.

A previous report showed that topoisomerase II inhibitors induced IFN-I pathway activation through the ATM and cGAS-STING pathway, which can prevent the Ebola virus infection (43). Consistent with these findings, teniposide induced IFN-I pathway activation both in tumor cells and tumor tissues depended on the cGAS-STING pathway, as knocked-out STING or cGAS blocked the IFN-I pathway activation. Intriguingly, a recent work reported that etoposide, another type of Top II inhibitor, elicited NF-κB activation through a STING-dependent but cGAS-independent fashion (44). In our study, teniposide-induced IFN-I activation required both cGAS and STING in tumor cells. Interestingly, a functional cGAS was also essential for tumor immunogenicity recognized by NK cell-mediated antitumor immunity (45). It is possible that etoposide and teniposide induced different signaling pathways that induce DNA damage, or they may have additional unknown targets besides topoisomerase II (46). Moreover, we observed that IFNAR receptor deficiency on DCs attenuated the activation of T cell. It indicated the essential role of IFN-I on DC activation in anti-tumor immune response. However, IFNAR deficiency did not completely inhibit T cell activation, suggesting that other innate immune signaling could be also involved in the DC activation and function.

Indeed, we also detected NF-κB activation in tumor cells following teniposide treatment, and NF-κB inhibition in tumor cells by knocking down IKKβ also attenuated teniposide-induced immunogenicity. NF-κB activation was required for tumor immunogenicity induced by RIPK1-mediated necroptosis (20). Furthermore, NF-κB signaling also controlled several IFN-I gene expression such as IFN-β (47). Together, teniposide was identified to be able to induce the activation of NF-κB and cGAS/STING-mediated IFN-I signaling in tumor cells, both of which contributed to enhanced tumor immunogenicity.

Although both NF-κB and IFN-I signaling have an immune-stimulating function, they also induce expression of inhibitory immune molecules such as PD-L1 (35, 47). We found that teniposide induced the PD-L1 expression on multiple tumor cells in vitro. In vivo experiment showed that teniposide treatment induced T cell infiltration and activation in the tumor microenvironment. Anti-PD1 treatment has shown a superior efficacy therapy on multiple tumor types, but the response rate is still much lower than desired. The non-responder tumors are often found with low intra-tumor T cell infiltration or PD-L1 expression and formed a “cold” microenvironment preventing T cell re-activation following anti-PD1 treatment (3). Therapies that can boost T cell infiltration or PD-L1 expression inside tumors may have the potential to convert an immune “cold” tumor to a “hot” tumor, thereby increasing the tumor response to PD-L1/PD1 blockade, and expanding the benefit of anti-PD1 therapy. Recent studies have shown that the CDK inhibitors abemaciclib and dinaciclib can potentiate antitumor immunity and enhance the efficacy of checkpoint blockade (16, 48). On the other hand, radiation therapy can also enhance the inhibition of tumor progress by checkpoint blockade therapy, but the effect was limited to specific tumor types (49-50). Here we demonstrated that teniposide in combination with anti-PD1 resulted in enhanced antitumor efficacy on several mouse tumor models.

Overall, our findings suggest that teniposide could induce both NF-κB activation and cGAS/STING-mediated IFN-I signaling within tumor cells, in turn eliciting tumor immunogenicity and activating tumor microenvironment, which could sensitize tumor response to anti-PD1 treatment. As several clinical trials testing the efficacy of chemo-immunotherapy based on ICD-inducing drugs and checkpoint blockade antibodies are ongoing, our findings provide a potential chemo-immunotherapeutic approach for cancer treatment by using teniposide in combination with anti-PD1 antibody, and suggest that a test of intratumoral STING expression may help predict patient response to such chemo-immunotherapy.

Methods

Mice and Reagents

Six- to eight-weeks-old female C57BL/6J and BALB/c mice were purchased from the Charles River Laboratory (Beijing, China). OT-I mice and *Ifnar*$^{-/-}$ mice were obtained from Jackson Laboratory. All the mice were maintained under specific pathogen-free conditions and in accordance with the animal experimental guidelines of Sun Yat-sen University. All the animal procedures were approved by the Institutional Animal Care and Use Committee of Sun Yat-sen University.

The B16 (C57BL/6 mouse melanoma), LSV174T (human colon adenocarcinoma), CT26 (BALB/c mouse colon adenocarcinoma), and HEK293 cell line were obtained from ATCC. MC38 (C57BL/6 mouse colon adenocarcinoma) was kindly gifted by Dr. Yang Xuanming at Shanghai Jiaotong University, Shanghai, China. B16-OVA cells were constructed by stably expressing ovalbumin cDNA on B16 cells. PDAC murine pancreatic cancer cells were derived from spontaneous pancreatic cancer tissues of *K-ras*(*G12D*); *Ink4a*/*Arf* $^{-/-}$ mice (51). DC2.4, a murine dendritic cell line, was kindly provided by Dr. Kenneth Dock at the University of Massachusetts Medical School, Worcester, MA. B3Z hybridoma cells were kindly gifted by Dr. Nilabh Shastri at the University of California, Berkeley, CA. All cell lines were tested as being mycoplasma free. The cells were maintained either with DMEM (Invitrogen) supplemented with 10% FBS and 1% penicillin-streptomycin or RPMI 1640 (Invitrogen) supplemented with 1% penicillin-streptomycin and 10% FBS in a humidified atmosphere at 37℃ and 5% CO_2.

For primary cell cultures, single-cell suspensions of mouse bone marrow cells were cultured in RPMI-1640 medium containing 10% fetal bovine serum, supplemented with 20 ng/ml GM-CSF and IL4 (Peprotech, 315-03, 214-14). The culture media was refreshed every 2

days. DMSO was from Sigma (D2650); TNFα was from Peprotech (315-01A); Birinapant (A4219), LCL161 (A3541), z-VAD-FMK (A1902), mitoxantrone (B2114), teniposide (A8532), etoposide (A1971), doxorubicin (A3966), daunorubicin (B1099), nec-1 (A4213), SP600125 (A4604), NAC (A8356) and Bay 117082 (A4210) were all purchased from Apexbio Inc. Anti-mouse PD1 antibody (Clone G4) was kindly provided by Dr. Lieping Chen (52).

LacZ activity measurement

The procedures for lacZ activity measurement were performed according to previously described protocols (53). Briefly, after activation, B3Z cells in the wells of a cell culture plate were lysed and freeze-thawed, and then added with 50 μL/well PBS containing 0.5% bovine serum albumin and 100 μL/well substrate solution (1 mg/mL chlorophenolred β-D-galactopyranoside) dissolved in β-galactosidase buffer. The plate was incubated at 37℃ for 12 to 18 hours till color development reached a proper level, followed by color intensity reading at 590 nm using a microtiter plate reader.

Gaussia Luciferase measurement

HMGB1-Gluc reporter was stably transfected into tumor cells by a lentiviral-based backbone and the stably transfected cells were treated with drugs for indicated time point(s). A 50 μL culture medium was collected from each sample to measure their luciferase activity by using the Renilla Luciferase assay (Promega，E2820) according to the manufacturer's instructions (54).

Detection of genomic DNA in cytosolic extracts

The procedure for genomic DNA detection in cytoplasm was performed as previously described (55). Cytosolic DNA was extracted and quantified via qPCR using the primer specific for genomic DNA (*Polg1*). The primer sequence of *polg1* was as follows: forward primer, 5'-GATGAATGGGCCTACCTTGA-3', and reverse primer, 5'-TGGGGTCCTGTTTCTACAGC-3'.

CRISPR/Cas9 Knockout and shRNA knockdown

STING-deficient and cGAS-deficient cells were constructed through the CRISPR (clustered regularly interspaced short palindromic repeats)/Cas9 system (56). The single-guide RNA (sgRNA) sequences were designed using the Optimized CRISPR Design (http://chopchop.cbu.uib.no/). The guide sequences used were 5′-GACGCAAAGATATCTCGGAGG-3′ for cGAS, 5′-GTACCTTGGTAGACAATGAGG-3′ for STING. The sgRNA was inserted into the LentiCRISPR v2 vector which also contain *Streptococcus pyogenes* Cas9 nuclease gene. The cells were transiently transfected with plasmids followed by selection with puromycin for 2 days, and then the knock out effect was confirmed by Western blot analysis of whole cell protein extracts.

Expression of IKKβ, TBK1 and IRF3 was knocked down by indicated shRNA in tumor cells. Briefly, shRNA lentiviral vectors were co-transfected with pspax2 and pMD2.G packaging plasmids in 293T cells. The supernatants were harvested 48 hours post-transfection and used for infection with tumor cells, followed by puromycin selection for 2 days. The knockdown effect was assessed by Western blot analysis of whole cell protein extracts.

Western blot, immunofluorescence, and immunohistochemistry

The procedures for protein sample preparation from cell cultures, protein quantification, Western blot, and data analyses were performed as previously described (57). The following antibodies were used for Western blot analyses: Gaussia (NEB, E8023), actin (Sigma, A3854), cGAS (CST, 31659), STING (CST, 13647), STAT1 (CST, 14994), p-STAT1 (CST, 9167), p-p65 (CST, 3036), p65 (CST, 8248), TBK1 (CST, 3504), p-IRF3 (CST, 29047), IRF3 (CST, 4302). Protein bands were visualized by chemiluminescence using an ECL detection kit (Thermo Scientific, 32106).

For immunofluorescence, the cells were fixed in 4% paraformaldehyde (PFA) in PBS during 20 minutes at room temperature (RT), washed twice with PBS, and permeabilized with 0.5% Triton X-100 in PBS for 10 minutes. After 2 additional washes, the cells were blocked with 2% BSA, 2% FBS in PBS (IFF) for 1 hour at RT. The cells were then incubated with γH2AX antibody (CST, 9718) in IFF at 4℃ overnight. They were then washed 3 times with PBS, each for 10 minutes, followed by incubation with FITC–conjugated secondary antibodies (CST, 4412), and 1 μg/ml of DAPI in IFF for 1 hour at RT. After that, the cells were washed again 3 times with PBS, and the slides were examined using a fluorescent microscopy.

For immunohistochemistry, the tissue sections were deparaffinized in xylene rehydrated by incubation in serial ethanol baths (95%-30%, 2 minutes per bath). Epitope retrieval was performed through incubation in 10 mM citrate buffer (pH=6.0) for 30-40 minutes. Endogenous peroxidase activity was inhibited by treatment with 3% H_2O_2 for 10 minutes. The tissue slides were then incubated for overnight at 4℃ with anti-CD8 (dilution: 1:200, CST, 70306) or anti-CRT (dilution: 1:100, Abcam, ab2907) primary antibodies. After washes in PBS, the slides were incubated for 30 minutes at RT with a secondary antibody (Dako), and the signal was subsequently detected by the chromogenic substrate (Dako)..

Detection of apoptosis, surface CRT staining, and LDH assay

Tumor cell lines were seeded in 24-well multiple plates, then treated with teniposide or DMSO for an indicated time point(s). Tenipside-induced tumor cell death was assessed using the Annexin V–Propidium Iodide Apoptosis Detection Kit (BD, 556547), detection of surface CRT (Abcam, ab2907) and measurement of the LDH release using the CytoTox96 Non-Radioactive assay kit (Promega, G1780). The procedures were performed following the kits' instructions. Briefly, LDH is a cytosolic soluble enzyme and will leak into culture medium when cells undergo cell death. Then the enzyme activity in the medium could be quantified by a colorimetrical assay.

T cells and DC cells activation assay

B16-OVA tumor cells were treated with teniposide for 16 hours. Treated tumor cells were then co-cultured with DC and T cells (B3Z or OT-I cells) for additional indicated time point(s). The LacZ activity was performed as previously described. Supernant levels of IL-2 and IFNγ were measured by ELISA kits (eBioscience, 88-7024-88, 88-7314-22). T cells were stained with fluorescence labeled antibodies against CD8 (eBioscience, 11-0081-82), CD69 (Biolegend, 104514), IFNγ (eBioscience, 25-7311-82), GZMB (eBioscience, 48-8898-82); DCs were stained with CD11c (eBioscience, 61-0114-82), MHC-II (eBioscience, 11-5321-82), CD40 (eBioscience, 12-0401-82), CD86 (eBioscience, 12-0862-82), CD80 (eBioscience, 46-0801-82), MHC-I (eBioscience, 48-5999-82), MHC-I SIINFEKL (eBioscience, 17-5743-80). After antibody staining, the cells were then analyzed using flow cytometry.

Real-time PCR and ELISA analysis

Total RNA was isolated using Trizol (Invitrogen, 15596018) according to the manufacturer's instructions. RNA was reversely transcribed using Primer Script Revers Transcriptase reagent Kit with gDNA Eraser (Takara, RR036A). Real-time PCR was performed using the SYBR Premix kit (Genstar, A301), and analyzed using the Bio-Rad CFX96 thermal cycler. The primer sequences used for the investigated mouse genes were as followed: actin-F: 5'-AGAGGGAAATCGTGCGTGAC-3', actin-R: 5'-CAATAGTGATGACCTGGCCGT; CCL5-F: GCTGCTTTGCCTACCTCTCC-3', CCL5-R: 5'-TCGAGTGACAAACACGACTGC-3'; CXCL10-F: 5'-CCAAGTGCTGCCGTCATTTTC-3', CXCL10-R: 5'-GGCTCGCAGGGATGATTTCAA-3'; IFNβ-F: 5'-CAGCTCCAAGAAAGGACGAA-3', IFNβ-R: 5'-GGCAGTGTAACTCTTCTGCAT-3'.

Supernatant levels of CCL5 and CXCL10 were measured by ELISA kits (R&D systems, DY478, DY466) following the manufacturer's instructions.

Tumor growth and treatments, and analytics

For the immunization study, 3×10^6 of CT26 cells, either freeze-thawed 3 times in liquid nitrogen or treated with 50 μM teniposide or 50 μM etoposide, were inoculated subcutaneously into the lower left flank of BALB/c mice. Eight days later, 5×10^5 live CT26 cells were inoculated into the right flank, and the tumor growth was monitored. For immunophenotyping analysis of tumor microenvironment, CT26 (5×10^5 cells) or B16 (1×10^6 cells) tumor cells were subcutaneously injected into the flank of BALB/c or B6 mice. Tumors were allowed to grow for 6-7 days and teniposide (dissolved in 10% Cremophor® EL in PBS, Sigma) or vehicle was administered by i.p. injection (10 mg/kg) twice at indicated time point(s). For analysis of immune cell populations, mouse tumors were dissociated by gentleMACS (Miltenyi Biotec) and filtered

through 70 μm cell strainers to generate single-cell suspensions, then stained with CD45 (eBioscience, 48-0451-82), CD3 (eBioscience, 46-0031-82), CD4 (eBioscience, 47-0041-82), CD8 (eBioscience, 11-0081-82), CD69 (Biolegend, 104514), IFNγ (eBioscience, 25-7311-82), GZMB (eBioscience, 12-8898-82) and TNFα (eBiosicence, 17-7321-82) for T cell analysis; Stained with CD11c (eBioscience, 61-0114-82), MHC-II (eBioscience, 47-5321-82), CD86 (eBioscience, 11-0862-82), CD40 (eBioscience, 12-0401-82) and MHC-I (eBioscience, 48-5999-82) for DC analysis. Fluorescence data were acquired on a BD LSR Fortessa cytometer and analyzed using the FlowJo7.6.5. For in vivo study, the CT26 (5×10^5 cells), MC38 (1×10^6 cells) or PDAC (1×10^6 cells) tumor cells were subcutaneously injected into the flank of BALB/c or B6 mice. The growth of the tumors was observed for 6-7 days, then teniposide or vehicle was administered by i.p. injection (10mg/kg) twice at an indicated time point(s), and followed by three times i.p. injection of anti-PD1 (100 μg/mouse, once every 3 days). The tumor volume was calculated as $0.5\times$tumor length$\times$(tumor width)^2, where the longer dimension was considered as the tumor length.

Anti-CD4 (BE0003-1), anti-CD8 (BE0004-1) and isotype (BE0089) depletion antibodies were purchased from Bioxcell Inc. Depletion antibodies were i.p. injected on day 3, 6 and 9 after tumor inoculated in an amount of 100 μg/mice, and depletion effect was confirmed by flow cytometry.

Statistics

Data were analyzed using GraphPad Prism 5 (GraphPad Software). Comparisons between two groups were analyzed using a two-tailed unpaired Student's *t*-test; Comparisons between multiple groups were analyzed using one-way ANOVA with Bonferroni post-test, or 2-way

ANOVA with Bonferroni post-test for tumor growth study. Statistical significance was defined as a *P* value of less than 0.05.

Study approval

All the animal procedures were approved by the Institutional Animal Care and Use Committee of Sun Yat-sen University.

References

1. Topalian SL, Wolchok JD, Chan TA, Mellman I, Palucka K, Banchereau J, et al. Immunotherapy: The path to win the war on cancer? *Cell.* 2015;161(2):185-6.
2. Galluzzi L, Chan TA, Kroemer G, Wolchok JD, and Lopez-Soto A. The hallmarks of successful anticancer immunotherapy. *Sci Transl Med.* 2018;10(459).
3. Zou W, Wolchok JD, and Chen L. PD-L1 (B7-H1) and PD-1 pathway blockade for cancer therapy: Mechanisms, response biomarkers, and combinations. *Sci Transl Med.* 2016;8(328):328rv4.
4. Yan L, and Zhang W. Precision medicine becomes reality-tumor type-agnostic therapy. *Cancer Commun (Lond).* 2018;38(1):6.
5. Ansell SM, Lesokhin AM, Borrello I, Halwani A, Scott EC, Gutierrez M, et al. PD-1 blockade with nivolumab in relapsed or refractory Hodgkin's lymphoma. *The New England journal of medicine.* 2015;372(4):311-9.
6. Garon EB, Rizvi NA, Hui R, Leighl N, Balmanoukian AS, Eder JP, et al. Pembrolizumab for the treatment of non-small-cell lung cancer. *The New England journal of medicine.* 2015;372(21):2018-28.
7. Chen L, and Han X. Anti-PD-1/PD-L1 therapy of human cancer: past, present, and future. *The Journal of clinical investigation.* 2015;125(9):3384-91.
8. Rizvi NA, Hellmann MD, Snyder A, Kvistborg P, Makarov V, Havel JJ, et al. Cancer immunology. Mutational landscape determines sensitivity to PD-1 blockade in non-small cell lung cancer. *Science.* 2015;348(6230):124-8.
9. Ayers M, Lunceford J, Nebozhyn M, Murphy E, Loboda A, Kaufman DR, et al. IFN-gamma-related mRNA profile predicts clinical response to PD-1 blockade. *The Journal of clinical investigation.* 2017;127(8):2930-40.
10. Turajlic S, Litchfield K, Xu H, Rosenthal R, McGranahan N, Reading JL, et al. Insertion-and-deletion-derived tumour-specific neoantigens and the immunogenic phenotype: a pan-cancer analysis. *The Lancet Oncology.* 2017;18(8):1009-21.
11. Overman MJ, Lonardi S, Wong KYM, Lenz HJ, Gelsomino F, Aglietta M, et al. Durable Clinical Benefit With Nivolumab Plus Ipilimumab in DNA Mismatch Repair-Deficient/Microsatellite Instability-High

559 Metastatic Colorectal Cancer. *Journal of clinical oncology : official journal of the American Society of*
560 *Clinical Oncology*. 2018;36(8):773-9.
561 12. Pfirschke C, Engblom C, Rickelt S, Cortez-Retamozo V, Garris C, Pucci F, et al. Immunogenic
562 Chemotherapy Sensitizes Tumors to Checkpoint Blockade Therapy. *Immunity*. 2016;44(2):343-54.
563 13. Galluzzi L, Buque A, Kepp O, Zitvogel L, and Kroemer G. Immunogenic cell death in cancer and
564 infectious disease. *Nature reviews Immunology*. 2017;17(2):97-111.
565 14. Casares N, Pequignot MO, Tesniere A, Ghiringhelli F, Roux S, Chaput N, et al. Caspase-dependent
566 immunogenicity of doxorubicin-induced tumor cell death. *The Journal of experimental medicine.*
567 2005;202(12):1691-701.
568 15. Mattarollo SR, Loi S, Duret H, Ma Y, Zitvogel L, and Smyth MJ. Pivotal role of innate and adaptive
569 immunity in anthracycline chemotherapy of established tumors. *Cancer research.* 2011;71(14):4809-20.
570 16. Hossain DMS, Javaid S, Cai M, Zhang C, Sawant A, Hinton M, et al. Dinaciclib induces immunogenic cell
571 death and enhances anti-PD1-mediated tumor suppression. *The Journal of clinical investigation.*
572 2018;128(2):644-54.
573 17. Menger L, Vacchelli E, Adjemian S, Martins I, Ma Y, Shen S, et al. Cardiac glycosides exert anticancer
574 effects by inducing immunogenic cell death. *Sci Transl Med.* 2012;4(143):143ra99.
575 18. Obeid M, Tesniere A, Ghiringhelli F, Fimia GM, Apetoh L, Perfettini JL, et al. Calreticulin exposure
576 dictates the immunogenicity of cancer cell death. *Nature medicine.* 2007;13(1):54-61.
577 19. Michaud M, Martins I, Sukkurwala AQ, Adjemian S, Ma Y, Pellegatti P, et al. Autophagy-dependent
578 anticancer immune responses induced by chemotherapeutic agents in mice. *Science.* 2011;334(6062):1573-
579 7.
580 20. Yatim N, Jusforgues-Saklani H, Orozco S, Schulz O, Barreira da Silva R, Reis e Sousa C, et al. RIPK1 and
581 NF-kappaB signaling in dying cells determines cross-priming of CD8(+) T cells. *Science.*
582 2015;350(6258):328-34.
583 21. Sistigu A, Yamazaki T, Vacchelli E, Chaba K, Enot DP, Adam J, et al. Cancer cell-autonomous
584 contribution of type I interferon signaling to the efficacy of chemotherapy. *Nature medicine.*
585 2014;20(11):1301-9.

22. Zappasodi R, Merghoub T, and Wolchok JD. Emerging Concepts for Immune Checkpoint Blockade-Based Combination Therapies. *Cancer Cell.* 2018;34(4):690.

23. Yang H, Ma Y, Chen G, Zhou H, Yamazaki T, Klein C, et al. Contribution of RIP3 and MLKL to immunogenic cell death signaling in cancer chemotherapy. *Oncoimmunology.* 2016;5(6):e1149673.

24. Ma Y, Pitt JM, Li Q, and Yang H. The renaissance of anti-neoplastic immunity from tumor cell demise. *Immunol Rev.* 2017;280(1):194-206.

25. Sukkurwala AQ, Adjemian S, Senovilla L, Michaud M, Spaggiari S, Vacchelli E, et al. Screening of novel immunogenic cell death inducers within the NCI Mechanistic Diversity Set. *Oncoimmunology.* 2014;3:e28473.

26. Kepp O, Senovilla L, Vitale I, Vacchelli E, Adjemian S, Agostinis P, et al. Consensus guidelines for the detection of immunogenic cell death. *Oncoimmunology.* 2014;3(9):e955691.

27. Deng L, Liang H, Xu M, Yang X, Burnette B, Arina A, et al. STING-Dependent Cytosolic DNA Sensing Promotes Radiation-Induced Type I Interferon-Dependent Antitumor Immunity in Immunogenic Tumors. *Immunity.* 2014;41(5):843-52.

28. Woo SR, Fuertes MB, Corrales L, Spranger S, Furdyna MJ, Leung MY, et al. STING-dependent cytosolic DNA sensing mediates innate immune recognition of immunogenic tumors. *Immunity.* 2014;41(5):830-42.

29. Dou Z, Ghosh K, Vizioli MG, Zhu J, Sen P, Wangensteen KJ, et al. Cytoplasmic chromatin triggers inflammation in senescence and cancer. *Nature.* 2017;550(7676):402-6.

30. Gluck S, Guey B, Gulen MF, Wolter K, Kang TW, Schmacke NA, et al. Innate immune sensing of cytosolic chromatin fragments through cGAS promotes senescence. *Nature cell biology.* 2017;19(9):1061-70.

31. Ebert PJR, Cheung J, Yang Y, McNamara E, Hong R, Moskalenko M, et al. MAP Kinase Inhibition Promotes T Cell and Anti-tumor Activity in Combination with PD-L1 Checkpoint Blockade. *Immunity.* 2016;44(3):609-21.

32. Martins I, Kepp O, Schlemmer F, Adjemian S, Tailler M, Shen S, et al. Restoration of the immunogenicity of cisplatin-induced cancer cell death by endoplasmic reticulum stress. *Oncogene.* 2011;30(10):1147-58.

33. McKenzie JA, Mbofung RM, Malu S, Zhang M, Ashkin E, Devi S, et al. The Effect of Topoisomerase I Inhibitors on the Efficacy of T-Cell-Based Cancer Immunotherapy. *J Natl Cancer Inst.* 2018;110(7):777-86.

34. Woo SR, Corrales L, and Gajewski TF. Innate immune recognition of cancer. *Annu Rev Immunol.* 2015;33:445-74.

35. Zitvogel L, Galluzzi L, Kepp O, Smyth MJ, and Kroemer G. Type I interferons in anticancer immunity. *Nature reviews Immunology.* 2015;15(7):405-14.

36. Bald T, Landsberg J, Lopez-Ramos D, Renn M, Glodde N, Jansen P, et al. Immune cell-poor melanomas benefit from PD-1 blockade after targeted type I IFN activation. *Cancer discovery.* 2014;4(6):674-87.

37. Burnette BC, Liang H, Lee Y, Chlewicki L, Khodarev NN, Weichselbaum RR, et al. The efficacy of radiotherapy relies upon induction of type i interferon-dependent innate and adaptive immunity. *Cancer research.* 2011;71(7):2488-96.

38. Fu J, Kanne DB, Leong M, Glickman LH, McWhirter SM, Lemmens E, et al. STING agonist formulated cancer vaccines can cure established tumors resistant to PD-1 blockade. *Sci Transl Med.* 2015;7(283):283ra52.

39. Corrales L, Glickman LH, McWhirter SM, Kanne DB, Sivick KE, Katibah GE, et al. Direct Activation of STING in the Tumor Microenvironment Leads to Potent and Systemic Tumor Regression and Immunity. *Cell Rep.* 2015;11(7):1018-30.

40. Ahn J, Xia T, Rabasa Capote A, Betancourt D, and Barber GN. Extrinsic Phagocyte-Dependent STING Signaling Dictates the Immunogenicity of Dying Cells. *Cancer Cell.* 2018;33(5):862-73 e5.

41. Pantelidou C, Sonzogni O, De Oliveria Taveira M, Mehta AK, Kothari A, Wang D, et al. PARP Inhibitor Efficacy Depends on CD8(+) T-cell Recruitment via Intratumoral STING Pathway Activation in BRCA-Deficient Models of Triple-Negative Breast Cancer. *Cancer Discov.* 2019;9(6):722-737

42. Xia T, Konno H, Ahn J, and Barber GN. Deregulation of STING Signaling in Colorectal Carcinoma Constrains DNA Damage Responses and Correlates With Tumorigenesis. *Cell Rep.* 2016;14(2):282-97.

43. Luthra P, Aguirre S, Yen BC, Pietzsch CA, Sanchez-Aparicio MT, Tigabu B, et al. Topoisomerase II Inhibitors Induce DNA Damage-Dependent Interferon Responses Circumventing Ebola Virus Immune Evasion. *mBio.* 2017;8(2):pii: e00368-17.

44. Dunphy G, Flannery SM, Almine JF, Connolly DJ, Paulus C, Jonsson KL, et al. Non-canonical Activation of the DNA Sensing Adaptor STING by ATM and IFI16 Mediates NF-kappaB Signaling after Nuclear DNA Damage. *Mol Cell.* 2018;71(5):745-60 e5.

45. Marcus A, Mao AJ, Lensink-Vasan M, Wang L, Vance RE, and Raulet DH. Tumor-Derived cGAMP Triggers a STING-Mediated Interferon Response in Non-tumor Cells to Activate the NK Cell Response. *Immunity.* 2018;49(4):754-63 e4.

46. Pommier Y. Drugging topoisomerases: lessons and challenges. *ACS Chem Biol.* 2013;8(1):82-95.

47. Taniguchi K, and Karin M. NF-kappaB, inflammation, immunity and cancer: coming of age. *Nat Rev Immunol.* 2018;18(5):309-24.

48. Goel S, DeCristo MJ, Watt AC, BrinJones H, Sceneay J, Li BB, et al. CDK4/6 inhibition triggers anti-tumour immunity. *Nature.* 2017;548(7668):471-5.

49. Shaverdian N, Lisberg AE, Bornazyan K, Veruttipong D, Goldman JW, Formenti SC, et al. Previous radiotherapy and the clinical activity and toxicity of pembrolizumab in the treatment of non-small-cell lung cancer: a secondary analysis of the KEYNOTE-001 phase 1 trial. *The Lancet Oncology.* 2017;18(7):895-903.

50. Ko EC, Raben D, and Formenti SC. The Integration of Radiotherapy With Immunotherapy for the Treatment of Non-Small Cell Lung Cancer. *Clinical cancer research.* 2018;24(23):5792-5806.

51. Ling J, Kang Y, Zhao R, Xia Q, Lee DF, Chang Z, et al. KrasG12D-induced IKK2/beta/NF-kappaB activation by IL-1alpha and p62 feedforward loops is required for development of pancreatic ductal adenocarcinoma. *Cancer Cell.* 2012;21(1):105-20.

52. Hirano F, Kaneko K, Tamura H, Dong H, Wang S, Ichikawa M, et al. Blockade of B7-H1 and PD-1 by monoclonal antibodies potentiates cancer therapeutic immunity. *Cancer Res.* 2005;65(3):1089-96.

53. Lee YR, Yang IH, Lee YH, Im SA, Song S, Li H, et al. Cyclosporin A and tacrolimus, but not rapamycin, inhibit MHC-restricted antigen presentation pathways in dendritic cells. *Blood.* 2005;105(10):3951-5.

54. Wang Z, Ji J, Peng D, Ma F, Cheng G, and Qin FX. Complex Regulation Pattern of IRF3 Activation Revealed by a Novel Dimerization Reporter System. *Journal of immunology.* 2016;196(10):4322-30.

55. West AP, Khoury-Hanold W, Staron M, Tal MC, Pineda CM, Lang SM, et al. Mitochondrial DNA stress primes the antiviral innate immune response. *Nature.* 2015;520(7548):553-7.

56. Sanjana NE, Shalem O, and Zhang F. Improved vectors and genome-wide libraries for CRISPR screening. *Nat Methods.* 2014;11(8):783-4.

57. Peng D, Wang Z, Huang A, Zhao Y, and Qin FX. A Novel Function of F-Box Protein FBXO17 in Negative Regulation of Type I IFN Signaling by Recruiting PP2A for IFN Regulatory Factor 3 Deactivation. *Journal of immunology*. 2017;198(2):808-19.

Author contributions

ZW and XX conceived and designed the study. ZW conducted most experiments and wrote the manuscript. JC, HZ, FX, XW, JH, ML, WHL performed parts of the involved experiments. GZ, PZ, PH, LX, SC, WL provided reagents and analyzed data. LX and XX supervised the project and contributed in writing the manuscript.

Acknowledgments:

We thank Drs. Cliff Y Yang and Junchao Dong for critical reading of the manuscript, Dr. Jibin Li for statistical assistance, and Dr. Seeruttun Sharvesh Raj for language editing. This work was supported by the grants from National Key R&D Program of China (2018YFC1313300/2018YFC1313304 and 2017YFC0908503), the National Natural Science Foundation of China (Grants 81472578, 81773051, 81803005, 81572409), China Postdoctoral Science Foundation grant (2017M622884), the Guangdong Innovative and Entrepreneurial Research Team Program (2016ZT06S638), the Science and Technology Project of Guangdong Province (2017A020215031), and Guangdong Esophageal Cancer Institute (M201607).

The authors have no other relevant affiliations or financial involvement with any organization or entity with a financial interest in or financial conflict with the subject matter or materials discussed in the manuscript apart from those disclosed.

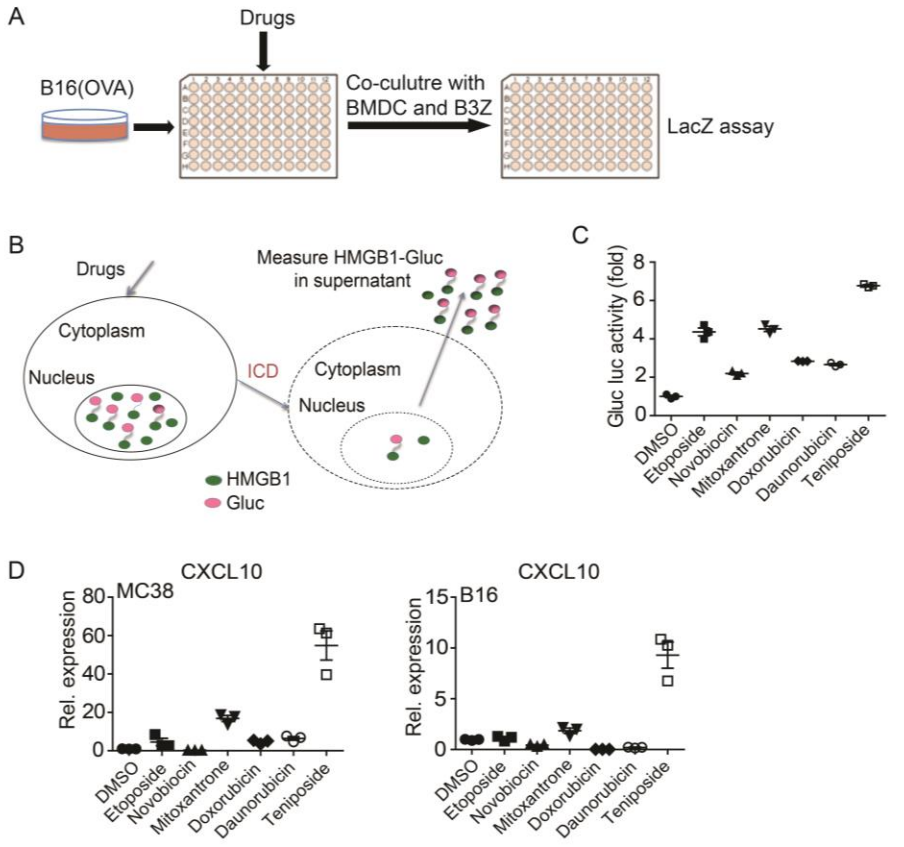

Figure 1. T cell-based drug screening identified novel immunogenic cell death inducers.

(**A**) An outline of drug screening protocol. B16-OVA tumor cells were seeded on 96-well plates and treated with drugs for 16 hrs, then co-cultured with BMDC and B3Z cells for 24 hrs. LacZ reporter activity was measured as a surrogate marker for T cell activation. (**B**) A cartoon illustrating the principle of the HMGB1-Gluc reporter system. Once drugs or inhibitors induce tumor cell ICD, HMGB1-Gluc will be released from nucleus into supernatant, and the supernatant luciferase activity would be detected. (**C**) MC38 (HMGB1-Gluc) cells were treated with different Top inhibitors or DMSO for 20 hrs, then the HMGB1-Gluc luciferase activity was measured. (**D**) MC38 and B16 cells were treated as in (**C**), and then the mRNA expression level of CXCL10 was measured by qPCR. Data in **C-D** are shown as mean ± SD of 3 independent experiments.

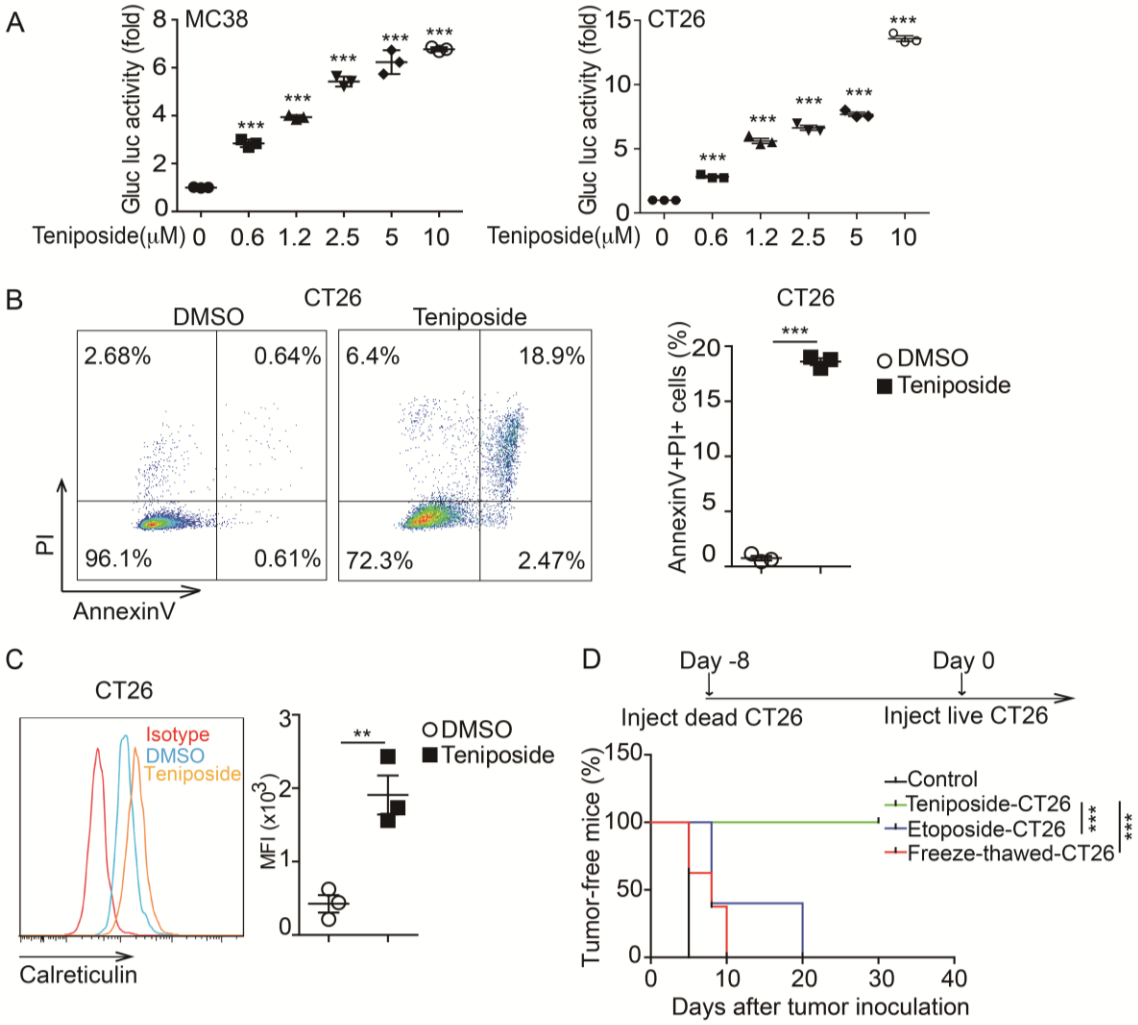

Figure 2. Teniposide induced immunogenic cell death of tumor cells.

(A) MC38 (HMGB1-Gluc) and CT26 (HMGB1-Gluc) cells were treated with increasing doses of teniposide for 20hr, and HMGB1-Gluc luciferase activity was measured. (**B-C**) CT26 cells were treated with teniposide or DMSO for 20 hrs, and the cell apoptosis (**B**) and surface expression of CRT(**C**) were detected by FACS. (**D**) CT26 tumor cells were pre-treated with teniposide, etoposide, or freeze-thawed, followed by subcutaneous inoculation into BALB/c mice as a vaccine (n=8 for Control group with no tumor cell vaccine administered, teniposide group and freeze-thawed group, and n=5 for etoposide group). After 8 days, mice were re-challenged with

live CT26 cells. Shown is the percentage of tumor-free mice 30 days post-re-challenge. Data in **A-C** are shown as mean ± SD of 3 independent experiments. $^{**}P < 0.01$, $^{***}P < 0.001$, by one-way ANOVA with Bonferroni post-test (**A)**, by unpaired Student's *t* test (**B)**, by log-rank (Mantel-Cox) test (**D)**.

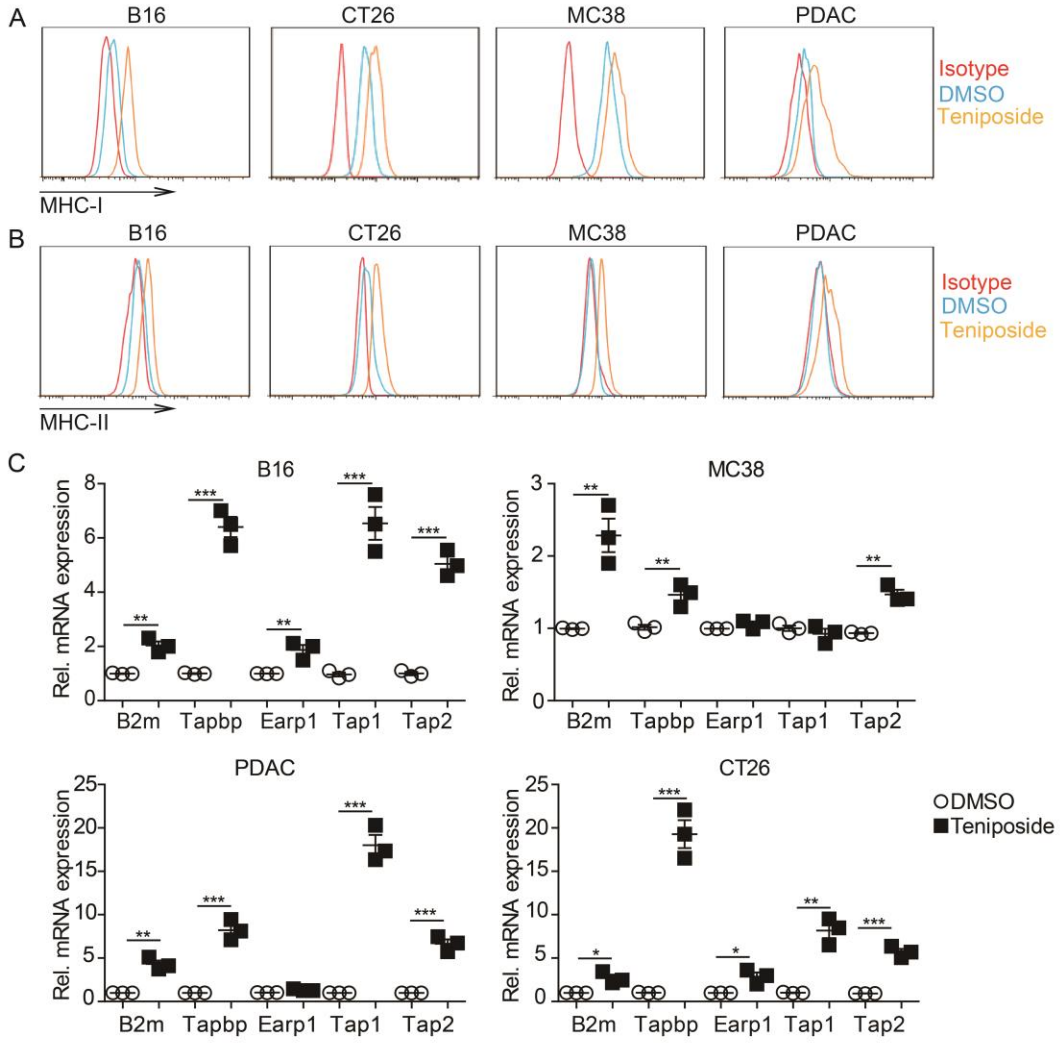

741

742 **Figure 3. Teniposide enhanced expression of antigen presenting machinery molecules on**

743 **tumor cells.**

744 (**A-B**) B16, MC38, PDAC and CT26 cells were treated with teniposide or DMSO for 20 hrs, and

745 the surface expression of MHC-I and MHC-II was determined by FACS. (**C**) Cells were treated

746 as in (**A**), and the expression of antigen presenting machinery genes were measured by qPCR.

747 Data in (**A-B)** are the representative result of 3 repeated experiments. Data in **C** are shown as

748 mean ± SD of 3 independent experiments. **P* < 0.05, ***P* < 0.01, ****P* < 0.001, by unpaired

749 Student's *t* test.

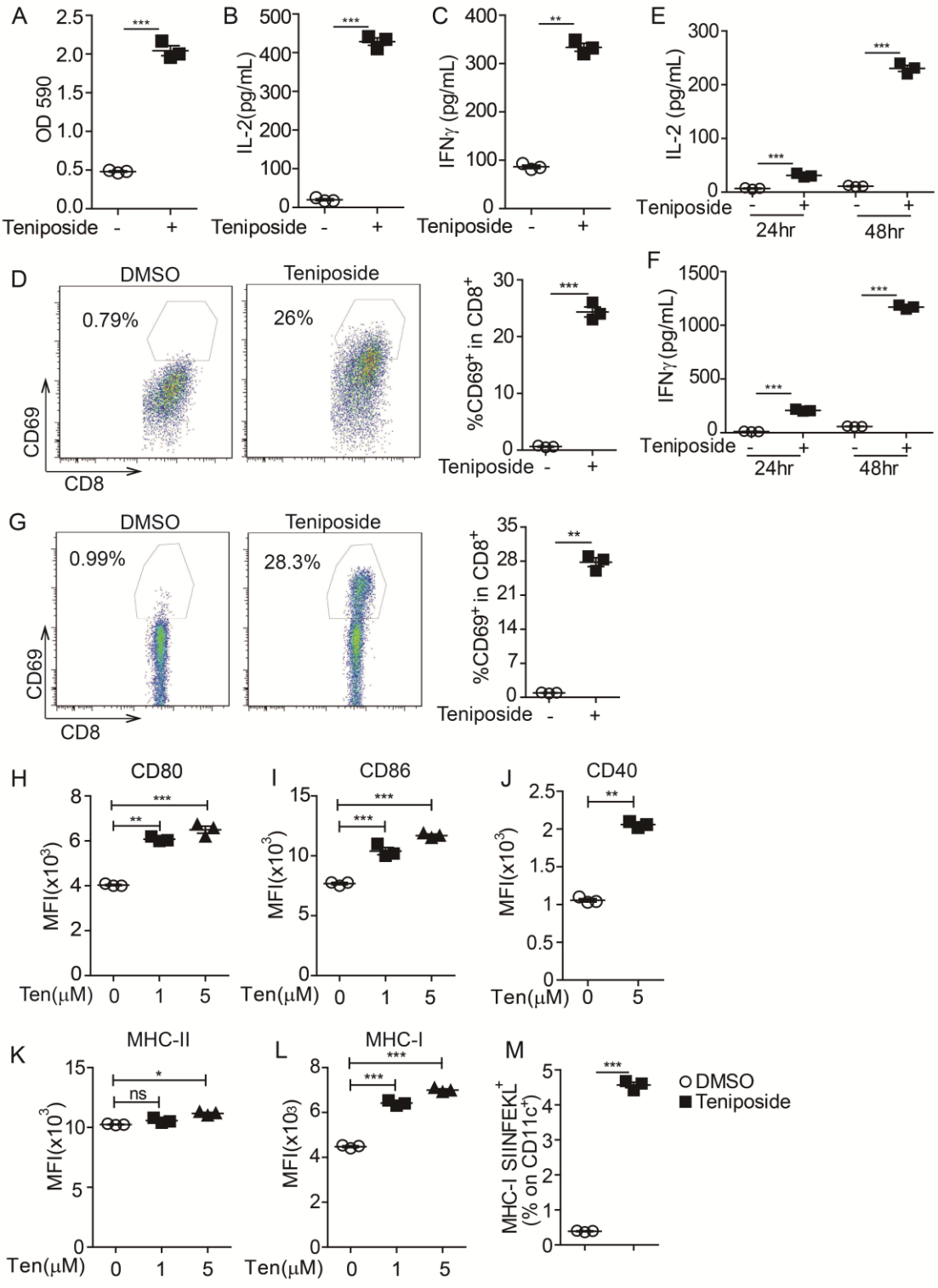

Figure 4. Teniposide-treated tumor cells induced T cell activation and dentritic cell maturation.

(**A-D**) B16-OVA cells were treated with teniposide or DMSO for 16 hrs, then co-cultured with BMDC and B3Z cells for additional 24 hr, then B3Z activation was measured by LacZ activity, IL-2 production and IFNγ production (**A-C**), and CD69 expression (**D**). (**E-G**) B16-OVA cells were treated with teniposide or DMSO for 16 hrs, then co-culture with BMDC and OT-I cells for additional 24hr or 48hrs, then the OT-I activation was measured by secretion of IL-2 and IFNγ, and surface expression of CD69. (**H-M**) B16-OVA cells were treated with DMSO or indicated concentration of teniposide for 16hrs and then co-cultured with BMDCs for additional 24 hrs, then the surface expression of CD80, CD86, CD40, MHC-II, MHC-I and MHC-I-SIINFEKL on CD11c+ DCs was determined by FACS. Data in (**A-M**) are shown as mean ± SD of 3 independent experiments. **P* < 0.05, ***P* < 0.01, ****P* < 0.001 and ns=not significant, by unpaired Student's *t* test (**A-G, J, M**); by one-way ANOVA with Bonferroni post-test (**H, I, K, L)**.

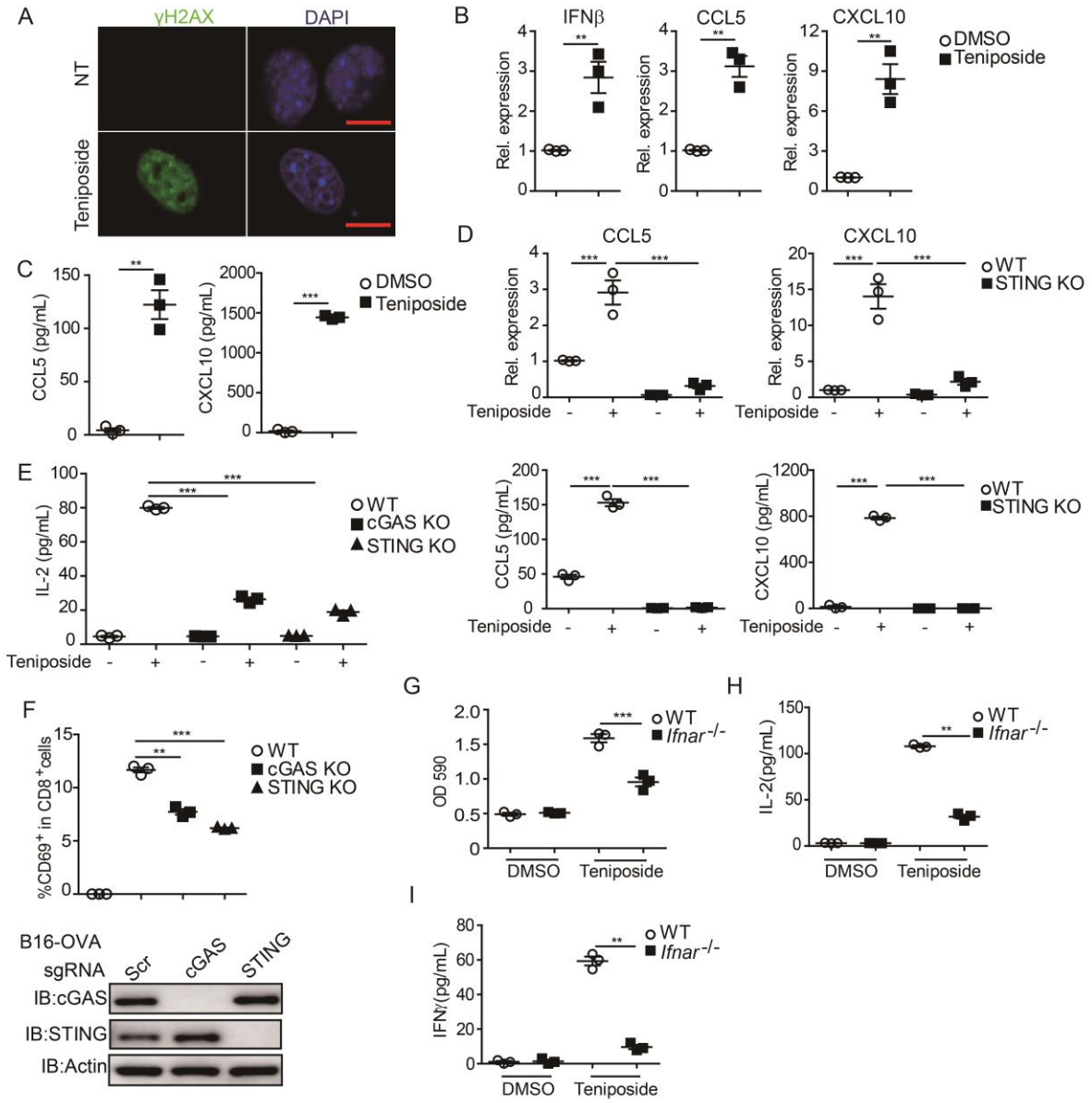

Figure 5. Teniposide activated cGAS/STING-dependent IFN-I signaling in tumor cells.

(**A**) B16 cells were treated teniposide or DMSO for 24 hrs, then γH2AX expression was detected by immunofluorescence staining. Scale bar: 10 μm. (**B**) B16 cells were treated as in (**A**), then the expression levels of IFNβ, CCL5 and CXCL10 was measured by qPCR. (**C**) Cells were treated as in **A**, then the supernatant levels of CCL5 and CXCL10 were measured by ELISA. (**D**) B16/WT and B16/STING KO cells were treated with teniposide or DMSO for 24 hrs, then the

levels of mRNA and protein expression of CCL5 and CXLC10 were measured by qPCR and ELISA, respectively. (**E-F**) B16-OVA/WT, B16-OVA/cGAS-KO and B16-OVA/STING-KO cells were treated with teniposide or DMSO for 16 hrs , then co-culture with B3Z+BMDCs for additional 24 hrs, and T cell activation was measured by supernatant IL-2 levels and surface expression of CD69; Lower panel, protein expression of cGAS or STING measured by Western blot; Actin was used as a loading control. (**G-I**) B16-OVA cells were treated with teniposide or DMSO for 16 hrs, then co-culture with B3Z in the presence of WT or *Ifnar*$^{-/-}$ BMDCs for additional 24 hrs, then LacZ activity and the supernatant levels of IL-2 and IFNγ were determined. Data in **A** are representative of one of 3 independent experiments. Data in (**B-I**) are shown as mean ± SD of 3 independent experiment. **P* < 0.05, ***P* < 0.01 and ****P* < 0.001, by unpaired Student's *t* test (**B-C**, **G-I**), by one-way ANOVA with Bonferroni post-test (**D-F**)**.**

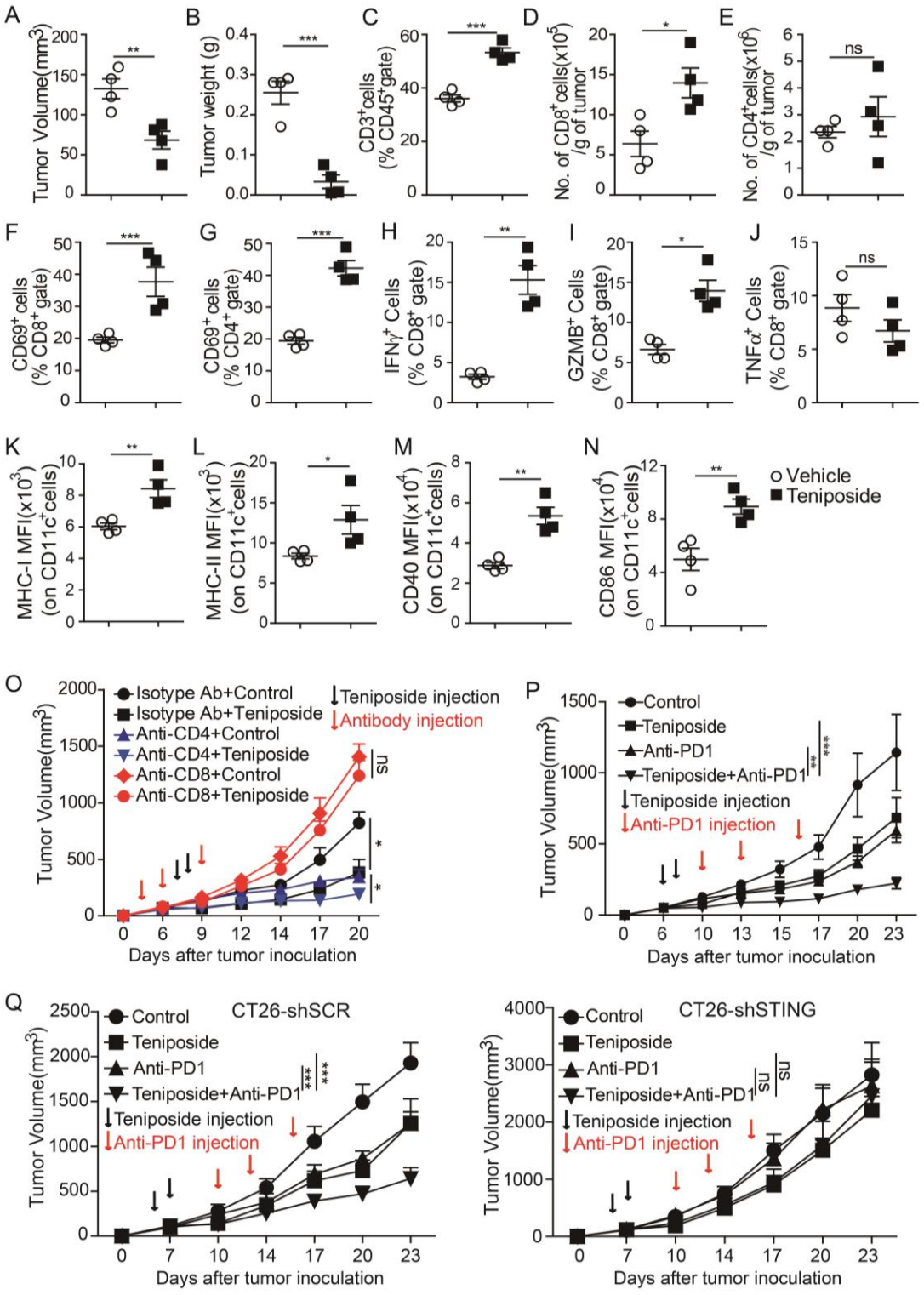

Figure 6. Teniposide induced immune cell infiltration and potentiated efficacy of anti-PD1 therapy on CT26 mouse tumor model.

(**A-N**) Mice with established CT26 tumors were treated with teniposide or vehicle on day 6 and 7 (10mg/kg, i.p.). Tumors were isolated on day 10, and tumor-infiltrating immune cells were analyzed by flow cytometry. Data are representative of one of two independent experiments. Shown are the tumor volume (**A**), tumor weight (**B**), intratumoral T cells (**C**), numbers of tumor-infiltrating CD8+ T cells (**D**), CD4+ T cells (**E**), and expression of activation marker CD69 (**F-G**) and effector molecules IFNγ, GZMB, TNFα (**H-J**) in CD8+ T cells. **(K-N)** Surface expression levels of MHC-I, MHCII, CD40, and CD86 on CD11c+ cells were determined by FACS**,** n=4 mice per group. (**O**) Mice were injected with CD8 or CD4 depletion antibody on day 3,6 and 9 after CT26 tumor inoculation, followed by teniposide treatment at day 7,8 (10mg/kg, i.p.). Tumor volume was shown as mean ±SD, n=5 per group. (**P**) Mice with established CT26 tumors were treated with teniposide, anti-PD1 or teniposide in combination with anti-PD1 at indicated time point(s). Tumor volume was shown as mean ±SD, n=7 per group. (**Q**) Mice were inoculated with CT26-shSCR (scramble shRNA as control) or CT26-shSTING cells, and then treated with indicated drugs. Tumor volume was shown as mean ±SD, n=5 per group. *$P < 0.05$, **$P < 0.01$, ***$P < 0.001$, ns=not significant, by unpaired Student's *t* test (**A-N**) or two-way ANOVA with Bonferroni post-test (**O-Q**).

833 **Table 1. The list of drugs elicited highest LacZ activity and HMGB1-Gluc activity**

Drugs	Bioactivity	LacZ activity	HMGB1-Gluc activity
Acrisorcin	Antifugal	2.21	11.5
Teniposide	Antineoplastic	2.12	5.97
Prednisolone tebutate	Antiinflammatory	2.06	1.44
Algestone acetophenide	Antiacne	1.82	1.38
Methscopolamine bromide	Anticholinergic	1.81	1.15
Flurandrenolide	Antiinflammatory	0.93	0.86

834